CONDENSED MATTER PHYSICS

Cooperative particle rearrangements facilitate the self-organized growth of colloidal crystal arrays on strain-relief patterns

Manodeep Mondal[1,2]*, Chandan K. Mishra[1], Rajdeep Banerjee[2,3], Shobhana Narasimhan[2,3], A. K. Sood[4,5], Rajesh Ganapathy[2,5]*

Strain-relief pattern formation in heteroepitaxy is well understood for particles with long-range attraction and is a routinely exploited organizational principle for atoms and molecules. However, for particles with short-range attraction such as colloids and nanoparticles, which form brittle assemblies, the mechanism(s) of strain-relief is not known. Here, we found that for colloids with short-range attraction, monolayer films on substrates with square symmetry could accommodate large compressive misfit strains through locally dewetted hexagonally ordered stripes. Unexpectedly, over a window of compressive strains, cooperative particle rearrangements first resulted in a periodic strain-relief pattern, which then guided the growth of laterally ordered defect-free colloidal crystals. Particle-resolved imaging of monomer dynamics on strained substrates also helped uncover cooperative kinetic pathways for surface transport. These processes, which substantially influenced the film morphology, have remained unobserved in atomic heteroepitaxy studies hitherto. Leaning on our findings, we developed a heteroepitaxy approach for fabricating hierarchically ordered surface structures.

INTRODUCTION

In the lattice-mismatched surface growth—heteroepitaxy—of metals and semiconductors, relaxation of the pent-up strain can result in surface reconstruction (*1*), the formation of periodic ripples (*2*), the nucleation of coherent three-dimensional (3D) islands (*3*), and the emergence of periodic arrays of dislocations (*4*, *5*). Apart from influencing the equilibrium film morphology, the strain also interferes with growth kinetics by altering energy barriers for interlayer (*6*) and intralayer (*7*–*10*) mass transport. The complex interplay of these processes, besides being of fundamental interest (*5*, *11*), often results in a high degree of self-organized growth and has also enabled the use of strain-relief patterns as templates for the large-area fabrication of ordered nanostructures composed of atoms (*4*, *12*), molecules (*13*), and even supramolecules (*14*). While there have been steady efforts to extend atomic epitaxy concepts to nanoparticles (*15*–*17*) and colloids (*18*–*23*) for creating functional surface structures, the high level of self-organization seen in atomic systems is yet to be achieved with these larger particles. It is only recently that the role of interparticle attraction range in surface growth processes is beginning to be appreciated. In DNA-functionalized nanoparticle heteroepitaxy (*17*), long-range interactions helped relax the misfit stress elastically and thin films grow pseudomorphically, i.e., in registry with the substrate, at ϵs, which in atomic heteroepitaxy would have invariably resulted in the formation of dislocations. Here, $\epsilon = \frac{a_s - a_f}{a_f}$ is the misfit strain with a_s and a_f being the lattice constants of the substrate and the film, respectively. On the other hand, for particles with short-range attraction (*24*, *25*), where the formation of topological defects is prohibitively energy expensive (*26*), the mechanism of strain-relief is not known. Short-range attractions are particularly interesting in the context of epitaxy because entropic effects promote nucleation of pseudomorphic crystal nuclei even for large ϵs (*21*). Short-range interactions modify kinetic processes even in colloidal homoepitaxy (*20*). Particle-resolved experiments have revealed that the barrier for interlayer mass transport in colloids is a diffusion-mediated pseudobarrier (*20*) and not a real energy barrier such as in atoms (*9*). Similar kinetic barriers were later observed to operate in the epitaxy of C_{60} molecules, which has an attraction range intermediate between atoms and colloids (*27*). Epitaxy processes carry over across particle size scales. Without prior knowledge of how strain modifies these processes, atomic/molecular kinetic Monte Carlo simulations, routinely used in surface growth studies, cannot accurately predict the film morphology (*11*). Evidently, there is a clear need for experiments that can directly probe single-particle dynamics that otherwise remain inaccessible in atomic/nanoparticle heteroepitaxy.

Motivated by these open issues, we investigated the heteroepitaxy of micrometer-sized colloids with short-range attraction. The ability to visualize and manipulate colloid dynamics at the single-particle level has been exploited in the past to shed light on a plethora of atomic phenomena that include glass transition (*28*), crystal melting (*29*, *30*), defect dynamics (*31*), homoepitaxy (*20*), and solid-solid transitions (*32*) to name a few. Here, we not only uncovered the mechanism of strain-relief for particles interacting through a short-range attraction but also show that the degree of the self-organized growth seen in atomic heteroepitaxy can be achieved in colloidal heteroepitaxy. Our particle-resolved bright-field optical microscopy experiments helped unveil cooperative particle dynamics that not only opened new kinetic pathways for monomers surface transport but also resulted in a strain-relief pattern that subsequently guided colloidal self-assembly.

[1]Chemistry and Physics of Materials Unit, Jawaharlal Nehru Centre for Advanced Scientific Research, Jakkur, Bangalore 560064, India. [2]School of Advanced Materials (SAMat), Jawaharlal Nehru Centre for Advanced Scientific Research, Jakkur, Bangalore 560064, India. [3]Theoretical Sciences Unit, Jawaharlal Nehru Centre for Advanced Scientific Research, Jakkur, Bangalore 560064, India. [4]Department of Physics, Indian Institute of Science, Bangalore 560012, India. [5]International Centre for Materials Science, Jawaharlal Nehru Centre for Advanced Scientific Research, Jakkur, Bangalore 560064, India.
*Corresponding author. Email: deep.manodeep10@gmail.com (M.M.); rajeshg@jncasr.ac.in (R.G.)

RESULTS

Strain-relief in colloidal heteroepitaxy

In our experiments, polystyrene colloids (diameter, $\sigma = 1$ μm) in the presence of a depletant (radius, $R_g \approx 50$ nm) were sedimented at constant flux, F, on patterned (100) substrates (Materials and Methods; fig. S1) (*33*). On (100) substrates, strain-relief by trivially forming stacking faults is forbidden (*18*, *34*). Upon deposition, monomers explored the surface by activated hopping to neighboring lattice sites (movie S1). We directly measured the particles' surface diffusion constant D through standard particle tracking procedures (*35*). Here, $D = D_o e^{-E_a/k_B T}$ where D_o is the attempt frequency, E_a is the activation barrier, and $k_B T$ is the thermal energy. While our experiments were largely done at a constant F, such as in atomic epitaxy, both D and F can be independently tuned in colloidal epitaxy as well (*20*). Our experiments were performed at constant F (section S3 and fig. S2). With time, the increase in particle surface coverage Θ led to the nucleation and growth of islands, which then coalesced to form films. We limit our attention to the post-island coalescence regime (see section S4 and fig. S3 for island growth precoalescence). We studied film growth for misfits that spanned from $\epsilon = -5.5\%$ (compressive strain) to $\epsilon = +5.5\%$ (tensile strain). The range of depletion bonds is $\sim 0.05 a_f$, and particles occupying adjacent substrate lattice sites can just about form in-plane bonds at the maximum ϵ studied. In addition to the strength of the interparticle attraction U, E_a can also depend on ϵ (*8*, *10*, *36*). To isolate the influence of ϵ on D, if any, U was held constant.

Representative snapshots of growth at $\Theta = \Theta_{onset}$, the coverage at which island nucleation began in the second layer, i.e., on top of the first monolayer/wetting layer, are shown in Fig. 1A. Particles in these images are labeled on the basis of their dominant local bond order parameters $|\psi_{4j}| = \frac{1}{N}\sum_{k=1}^{N} e^{4i\theta_{jk}}$ or $|\psi_{6j}| = \frac{1}{N}\sum_{k=1}^{N} e^{6i\theta_{jk}}$ (Fig. 1A and section S5). Here, θ_{jk} is the bond angle between particles j and k, and N is the number of the nearest neighbors of particle j. The misfit strongly influenced the structure and dynamics of the wetting layer. We quantified the degree to which the film wets the substrate through $w = \frac{N_{\psi_4}}{N_{\psi_4} + N_{\psi_6}}$, with $w = 1$ corresponding to complete wetting (pseudomorphic films) and $w = 0$ to complete dewetting. Here, N_{ψ_4} and N_{ψ_6} are the number of particles in islands with high fourfold and sixfold order, respectively. For $\epsilon = 0$, particles in the wetting layer were stable and in complete registry with the substrate (Fig. 1A), and w was independent of Θ. Unexpectedly, w evolves with Θ for $\epsilon \neq 0$ (Fig. 1C). With increasing tensile strain, although there was a concomitant enhancement in particle position fluctuations, the film was largely pseudomorphic with the substrate except at the largest ϵs, where we found a few isolated patches of close-packed crystals (Fig. 1A). While the film remained pseudomorphic for $\epsilon = -1.5\%$, at larger compressive misfits, we observed faceted domains of particles with high $|\psi_{4j}|$ separated by dewetted stripes of particles with a high $|\psi_{6j}|$. The width of these stripes fluctuated between one particle (for $\epsilon = -2.4$ and -4.4%) and one to three particles wide (for $\epsilon = -3.5$ and -5.5%) (Fig. 1, A and B). While an asymmetry in the growth for $-\epsilon$ and $+\epsilon$ is expected because of the asymmetry in the particle pair potential (*37*), the peaks and valleys in w, at a fixed Θ, for $\epsilon < 0$ are reminiscent of commensurate-incommensurate transitions seen in monolayers adsorbed on periodic potentials (*38*). Our attempts to capture this behavior by a 1D Frenkel-Kontorova model did not produce lowest-energy configurations that resembled experimental ones (section S6 and figs. S4 and S5).

By locally dewetting and forming stripes, the wetting layer could accommodate even large strains laterally. Such a mode of relaxation has been observed during the epitaxial growth of Cu on Ni(100) ($\epsilon = -2.6\%$) (*34*), and such as in this system, the stripes observed in our experiments never intersect or coalesce, are precisely one particle wide for nearly the same ϵ, and run along the ⟨110⟩ directions, which corresponds to the direction of maximum compressive stress for face-centered cubic (FCC)(100). This similarity between atomic and colloidal systems is probably because the spatial dependence of the repulsive part of the pair potential, which primarily influences the relaxation mechanism for $\epsilon < 0$, is not very different. We, however, note that the complex internal structure of the stripes seen at other ϵs has no parallel in atomic systems. The driving force behind the stripe formation stems from particles in the wetting layer trying to maximize their coordination. Because of the nearly hardcore nature of the repulsion, when the island reaches a threshold size that depends on ϵ, particles that make its perimeter cannot occupy the fourfold hollow sites of the underlying substrate. During island coalescence, by making a 0.5σ displacement along the island edge to the twofold bridge site of the substrate, these dewetted particles can form six in-plane bonds and two out-of-plane bonds and achieve the same total coordination as particles in the island interior—four in-plane and four out-of-plane bonds (Fig. 1D). On increasing the compressive strain, a decrease in the interstripe separation, keeping its width fixed, is not optimal to accommodate the misfit, and the stripe thickness varies with ϵ (fig. S6). This suggests that the overall film morphology is a tradeoff between bulk wetting and particles maximizing their local coordination.

Misfit strain alters intralayer monomer mobilities

Since F and U are held fixed in our study, the naive expectation that is Θ_{onset} should be independent of ϵ. This is however not the case (Fig. 1A). Θ_{onset} at all $\epsilon \neq 0$ is substantially larger than its $\epsilon = 0$ value and shows clear peaks and valleys for $\epsilon < 0$ (Fig. 2A, section S8, and fig. S7). This trend can only emerge if mainly D and, possibly, processes that govern monomer descent from island terraces are also altered by strain (*6*, *9*, *39*). Since the measured monomer diffusivities on the substrate did not reveal any misfit dependence (section S9 and fig. S8), it is the change in structure and dynamics of the wetting layer with ϵ that changes D, and possibly also their dynamics at island step edges. When $\epsilon < 0$, because of the coexistence of pseudomorphic domains and stripes, monomers diffusing on the wetting layer experience an inhomogeneous surface potential comprising fourfold and threefold hollow sites. Since E_a for threefold hollow sites is smaller than the fourfold ones, the spatially averaged D for $\epsilon < 0$ will be larger in comparison to its $\epsilon = 0$ value. Also, because of variations in the stripe thickness and, hence, the fraction of threefold hollow sites with decreasing ϵ, D also fluctuates (red squares in Fig. 2B). A close inspection of dynamics of the wetting layer further revealed that particles in pseudomorphic domains vibrate more for $\epsilon = -3.5$ and -5.5% than for $\epsilon = -2.4$ and -4.4% (movie S2). We isolated the role of vibrational entropy contributions toward D by directly measuring activation barriers, E_a^{sq}, and monomer mobilities, D_{sq}, only on the pseudomorphic regions of the wetting layer (sections S10 and S11). Both D_{sq} and E_a^{sq} once again show peaks and valleys coinciding with those seen in D (Fig. 2B). Thus, for certain misfits, pseudomorphic domains of a suitable size when decorated by stripes create stable particle packings in the wetting layer.

When $\epsilon > 0$, where the wetting layer is largely pseudomorphic with the substrate, D systematically increased with ϵ primarily due to the lowering of E_a from vibrational entropy contributions (Fig. 2B). In

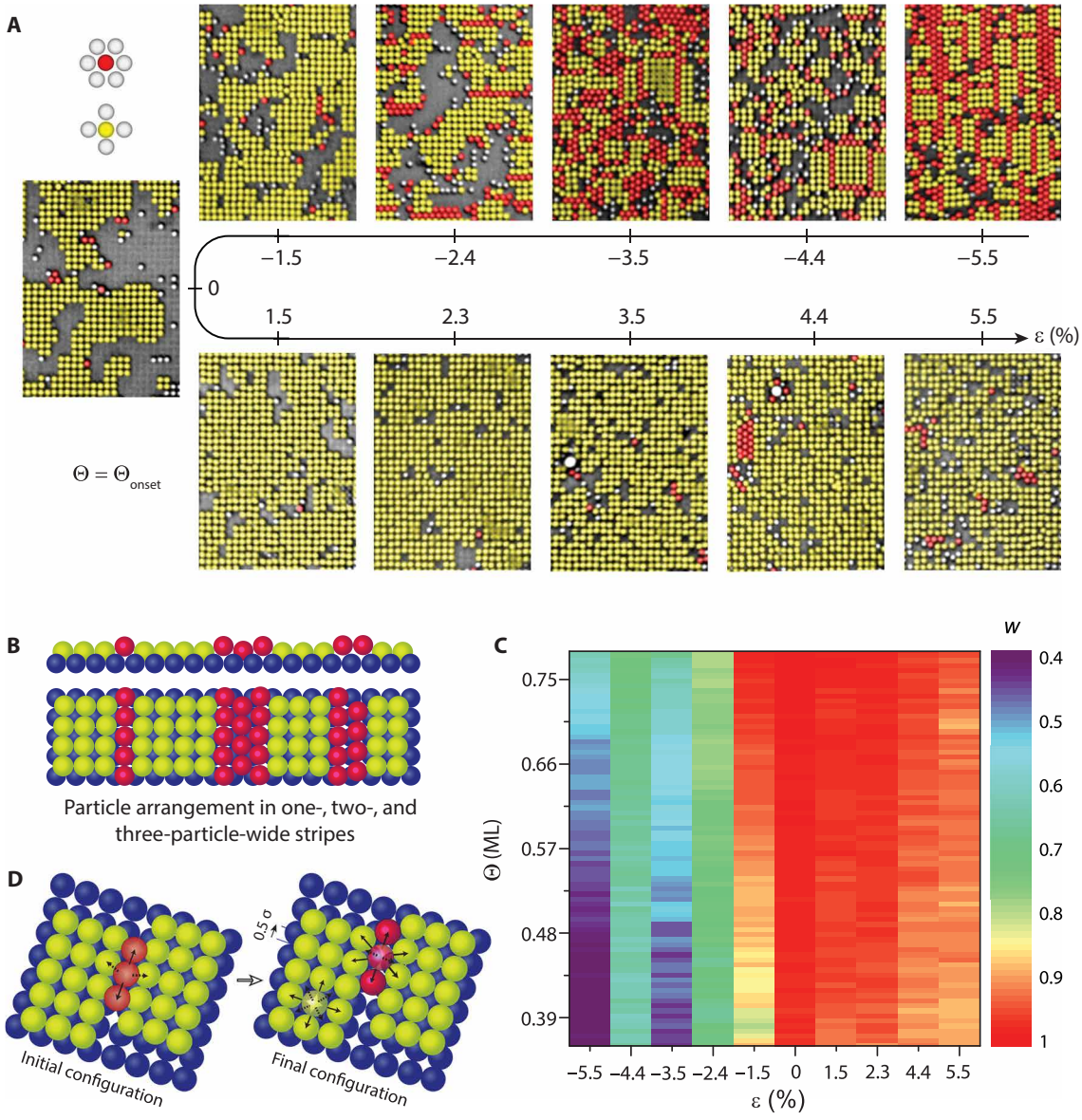

Fig. 1. Strain-relief in colloidal heteroepitaxy. (**A**) Snapshots of film growth at $\Theta = \Theta_{onset}$ at various ϵs. Particles are color coded based on their local bond order. Yellow and red colors represent fourfold and sixfold bond orders, respectively. (**B**) Schematic of particle order in stripes of different thicknesses. One- and two-particle-wide stripes had dewetted the substrate with their particles on the twofold bridge site. Three particle stripes had a row of particles in the fourfold hollow sites and were straddled by dewetted rows of particles that were located on the bridge site. (**C**) *w* as a function of Θ and ϵ. Colors represent the value of *w*. At fixed Θ, *w* versus ϵ shows clear peaks and valleys for compressive misfits. (**D**) Schematic shows that particles at the island perimeter (shown in red in the initial configuration) are squeezed out of the layer because of strain and cannot occupy the fourfold hollow site of the substrate (shown in blue). By sliding along the island edge by 0.5σ and occupying the bridge-site of the substrate, particles can form six in-plane and two out-of-plane bonds (denoted by solid and dashed black arrows, respectively). This is the same total coordination as particles in the island interior—four in-plane and four out-of-plane bonds.

atomic heteroepitaxy, E_a is usually larger for tensile than for compressive strains, as in the former, diffusing monomers not only see a more corrugated surface but can also form bonds with the subsurface layer due to the longer range of attractive interactions (*8*, *36*). The trend observed here is the opposite since attractive interactions here are short ranged, and vibrational entropy contributions smoothen out the surface corrugation and more so for tensile than for compressive strains. At large tensile misfits, direct imaging helped uncover yet another mode of diffusion enhancement, namely, "adcolloid" exchange. The sequence of images in Fig. 3A shows a monomer (indicated by a dashed circle in top left panel) dislodging a particle from the wetting layer below and occupying its position. The dislodged monomer subsequently occupied a fourfold hollow site adjacent to the original one (indicated by a full circle in bottom left panel), thus effectively counting as a particle hop (movie S3). Although indirect experimental evidence for adatom exchange came nearly three decades ago (*40*), direct visualization of this process and its intermediate steps in atomic systems have hitherto not been possible.

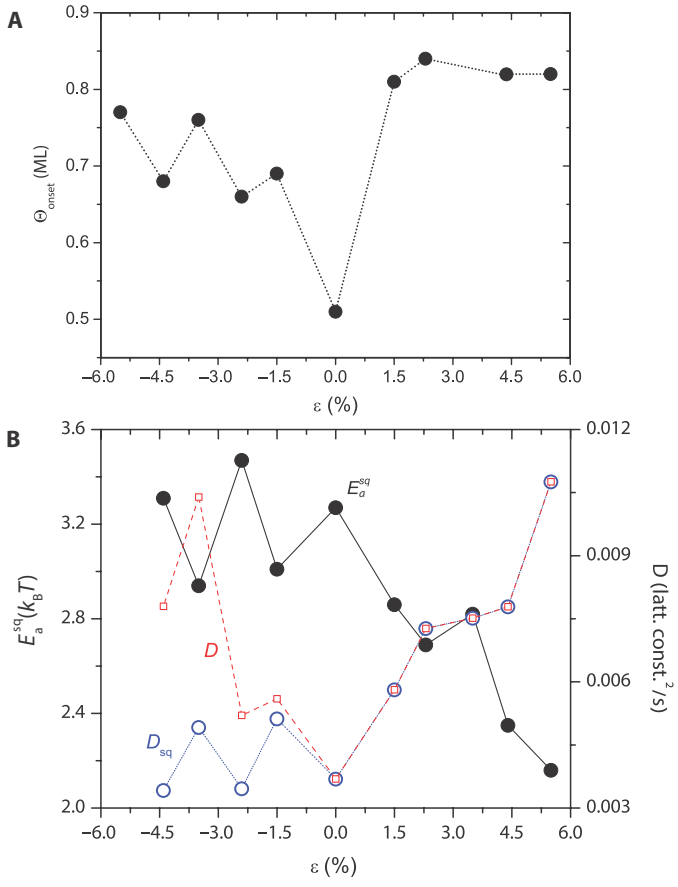

Fig. 2. Role of misfit strain on intra- and interlayer mass transport. (**A**) Θ_{onset} versus ϵ. (**B**) Monomer diffusivities and energy barriers E_a^{sq} versus ϵ. The hollow red squares denote the spatially averaged diffusivities on the wetting layer, and hollow blue circles correspond to particle diffusivities measured only on the pseudomorphic regions. The black circles represent the activation barrier E_a^{sq}.

Observation of new kinetic pathways for interlayer monomer transport

In addition to influencing *D*, the strain also modified the kinetics of monomer descent from island terraces. Previous colloidal homoepitaxy experiments noted that monomers diffuse a longer path to descend island step edges in comparison to that required for a hop between adjacent lattice sites in the island interior (*20*). Because the probability of returning to the origin in a 1D random walk scales with the path length (*41*), the longer descent path results in an increase in particle residence times, τ, at island step edges. This manifests as a pseudostep edge barrier that, nevertheless, assumes the role of a real energy barrier, with large τs promoting three-dimensional island growth rather than layer-by-layer growth. A clear indicator for the presence of a larger barrier is when the radius of islands R_c at $\Theta \approx \Theta_{onset}$ is smaller than the interisland spacing *L* at the onset of island coalescence (*9*, *20*, *42*). In our heteroepitaxy experiments, although the path length for step-edge descent remains nearly same with ϵ, we found that $R_c < L$ for ϵ = 0 and $R_c > L$ for ϵ ≠ 0 (section S12 and fig. S11). For compressive strains, the smaller τ, in comparison to its value for ϵ = 0, is a consequence of the underlying film structure. When pseudomorphic domains are decorated with stripes, particles descending step edges must break a single bond with a particle in the penultimate island row (Fig. 3B) in comparison to two bonds when ϵ = 0 (Fig. 3C). The probability of step-edge descent is, thus, higher in the former than in the latter (movie S4) and thereby also contributes to a larger Θ_{onset}. For ϵ > 0, besides direct step-edge descent, we observed new kinetic pathways for descending monomers that once again resulted in a small τ and a larger Θ_{onset}. The representative sequence of images, corresponding to an ϵ = 5.5% in Fig. 3D shows an adcolloid on an island step edge exchanging positions with a particle in the island corner (labeled 1), with the latter remaining attached to the step edge after the descent. The descent also indirectly involves the displacement of a second particle (labeled 2) along the island step edge. Although adatom step-edge descent by one-particle push-out exchange is known to occur in many materials systems (*39*) and has been predicted even for compound metal surfaces (*43*), these moves are thought to involve the motion of only a single island atom at the step edge. For ϵ > 4.4%, we evidenced adcolloid descent processes that involved a higher degree of particle cooperativity. Snapshots in Fig. 3 (E and F) show a particle on a step edge being incorporated into the island by two-particle and four-particle push-out exchange, respectively. Collectively, these observations directly show that many distinct processes (Figs. 2 and 3) contribute to the trend observed in Θ_{onset} with ϵ. While simulations have investigated some of these processes (*39*, *44*), but often consider them in isolation, disentangling their individual roles on film growth is difficult, if not impossible, in atomic/nanoparticle epitaxy.

Self-organized growth on strain-relief patterns and hybrid heteroepitaxy

At even higher coverages ($\Theta \gtrapprox 0.8$) and for a narrow range of $-4.2\% \leq \epsilon \leq -4.9\%$, an unexpected structural transition occurred in the wetting layer—we observed the emergence of a periodic strain-relief pattern (movie S5). For a representative ϵ = − 4.4% (middle panel in Fig. 4A), this emergent order is manifested as a peak in the structure factor *S*(*q*) at a *q* corresponding to the periodicity of pseudomorphic domains [see zoomed-in image of *S*(*q*) in the middle panel in Fig. 4A]. This peak in *S*(*q*) is either completely absent or very weak when ϵ changes substantially (left and right panels in Fig. 4A). With further particle deposition, this self-generated pattern acted as a template and guided the growth of laterally ordered defect-free three-dimensional pyramids (movie S6 and fig. S12). Further, this lateral ordering extends over hundreds of micrometers in each direction and appears to be limited only by the template uniformity (section S13 and fig. S13). Experiments done over a range of *F* for the same ϵ showed nearly identical patterns (section S14 and fig. S14).

Since a continuous wetting film is formed through the coalescence of domains that grew out from random locations on the substrate (movie S7), a periodic strain-relief pattern cannot arise without some level of particle cooperativity. We found that lateral ordering was mainly achieved through the abrupt and collective sliding motion of two neighboring rows of particles, one belonging to the stripe and the other a pseudomorphic domain, by ≈ 0.5σ (Fig. 4B and movie S8). In doing so, the bond orders in these two rows swap (bottom panel in Fig. 4B), with the net result being a transverse shift in the position of the stripe by 1σ and an increase in the size of one of the pseudomorphic domains, at the expense of the other, by the same amount. These cooperative moves allow for substantial restructuring of the wetting layer even in the later stages of growth. We determined the extent to which cooperative dynamics depends on ϵ. Particles that underwent displacements larger than 0.3σ over a time interval $t^* = 1$ s

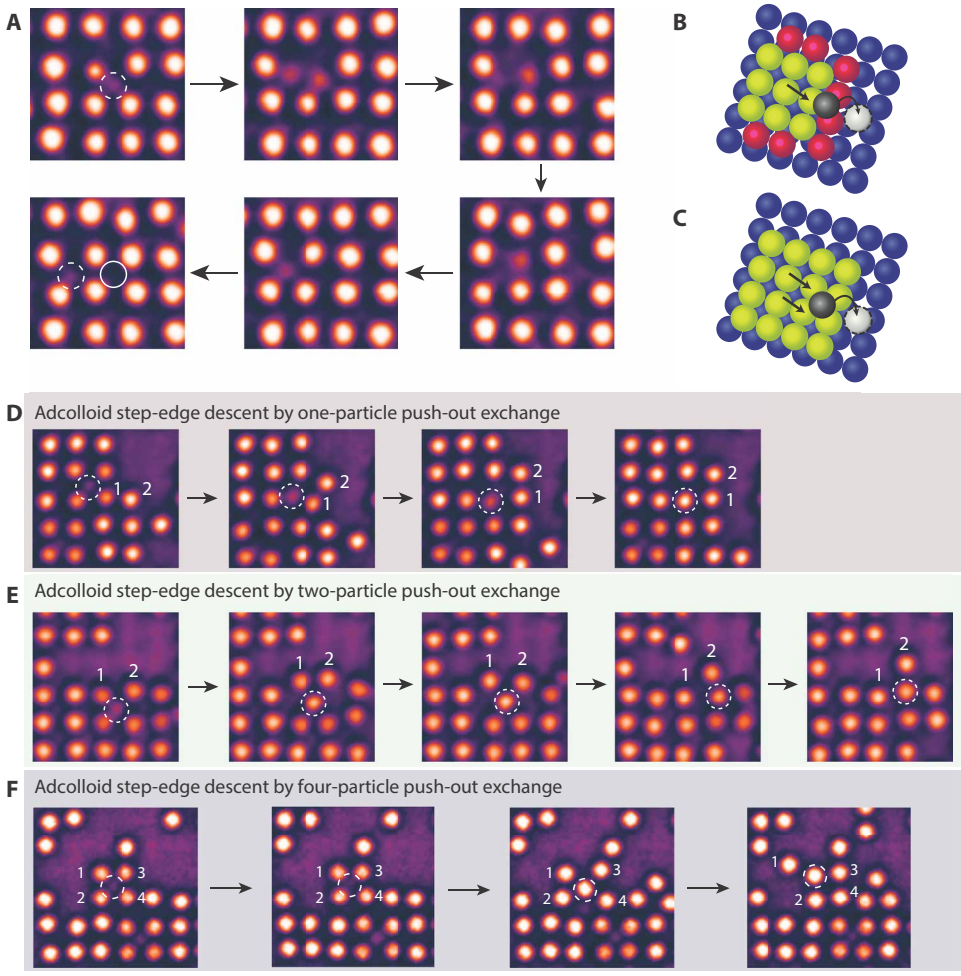

Fig. 3. Reaction pathways for intra- and interlayer mass transport. (**A**) Adcolloid exchange-mediated intralayer diffusion. The panels show the intermediate steps during this process. (**B**) Particle shown in gray attempting a step-edge descent for $\epsilon \leq -2.5\%$. Because of the hexagonally ordered stripe (red particles) at the island edge, the particle must break a single bond with the particle indicated by the arrow to descend the island terrace. (**C**) Particle shown in gray attempting a step-edge descent for $\epsilon = 0\%$. The particle must break two bonds to descend the step edge. (**D** to **F**) Adcolloids descending island terraces by one-particle, two-particle, and four-particle push-out exchange, respectively. The dashed circle represents the adcolloid, and the labeled particles correspond to those that aided in the descent. These moves are typically complete in 0.5 to 2 s.

were first identified and then clustered depending on whether they were nearest neighbors and moved cooperatively along the FCC (100) directions. The normalized histogram of cluster sizes $P(n)$ for $n \geq 3$, where n is the number of particles in a cluster, is shown in Fig. 4C. We defined an average cluster size as $P(n = \langle n \rangle) = 1/5$. $\langle n \rangle$ grows with $|\epsilon|$ and is larger for compressive than tensile strains (Fig. 4D). Although substantial cooperativity is present even for $\epsilon = -5.5\%$ and $\epsilon > 4.4\%$, lateral order is precluded in the former because of variations in the stripe thickness and in the latter by the nucleation of islands in the second layer, which resulted in complete dewetting of the film (section S15 and figs. S15 and S16). Epitaxy studies performed hitherto focus exclusively on monomer mobilities (*11*) and almost never consider cooperative dynamics during film growth. Our experiments show that this assumption, however, is appropriate only in the case of homoepitaxy.

Building on these observations, we demonstrate a new hybrid heteroepitaxy approach that brings together self-organized pattern formation with site-specific island nucleation to guide colloidal self-assembly. To achieve site-specific island nucleation, we designed strained (100) substrates ($\epsilon = -4.4\%$) and with periodically varying well depths, in this case Moiré patterns (section S16 and fig. S17) (*23*). The Moiré periodicity can be easily tuned in the fabrication step. Because of the geometric nature of our depletion interactions, periodic topographic gradients of the Moiré pattern manifest itself as periodic energy gradients for the diffusing colloids and helped transport particles to specific sites—"topotaxis" (*45*) of colloids. The enhancement in particle density at these sites resulted in island nucleation, which subsequently relaxed the misfit by forming stripes (Fig. 4E). At higher Θs, we observed a locally periodic strain-relief pattern, which was further organized at a larger length scale imposed by the Moiré periodicity. With continued particle deposition, the wetting layer once again acted as a template and led to the growth of hierarchically ordered defect-free 3D crystals.

DISCUSSION

In summary, our study has helped uncover a generic mechanism for strain-relief that circumvents the need to form topological defects in

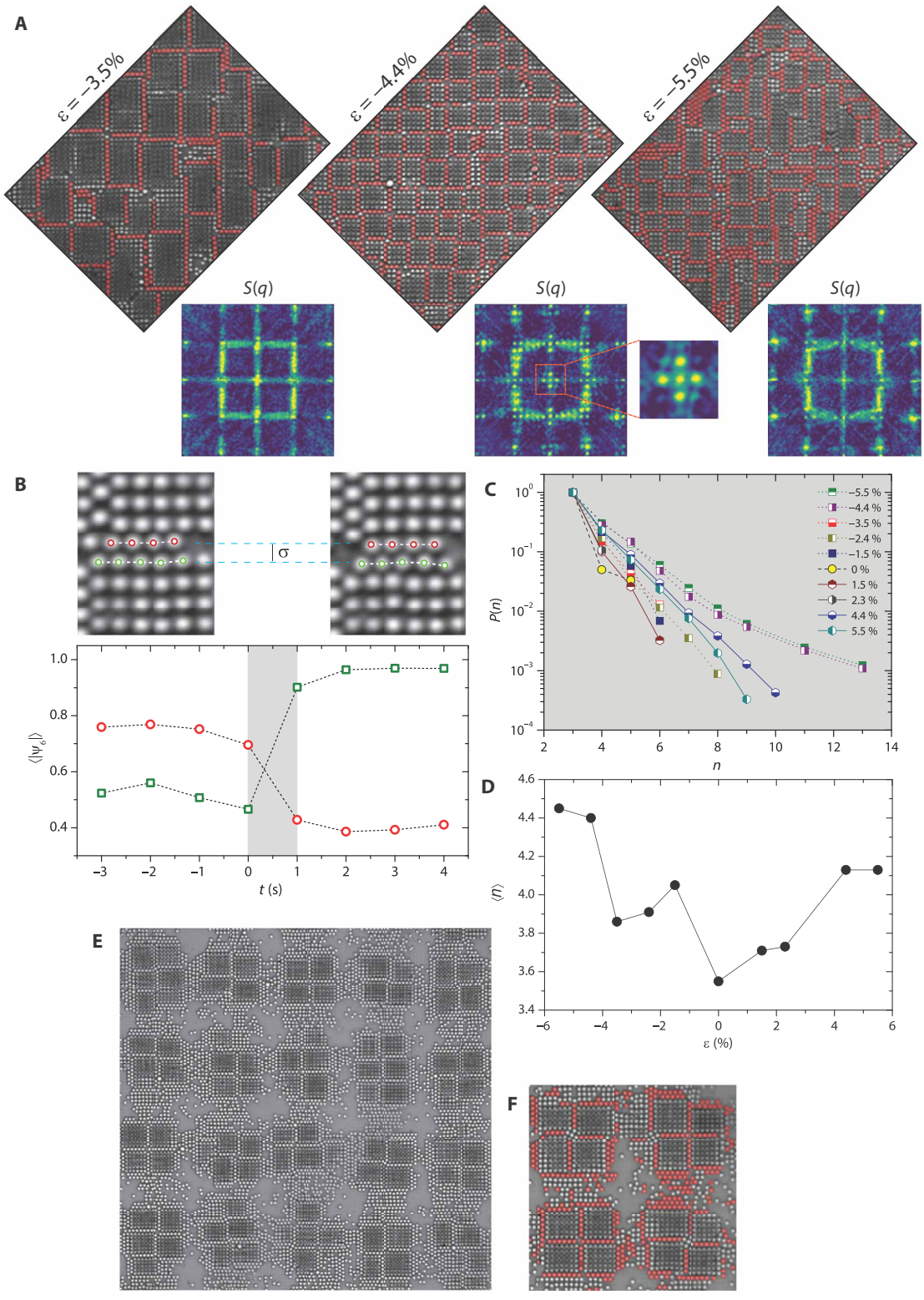

Fig. 4. Self-organized growth on strain-relief patterns and hybrid heteroepitaxy. (**A**) Snapshots of growth at various misfits. The particles labeled red have a high value of $|\psi_{6j}|$. The panels below represent $S(q)$. The periodicity of the pseudomorphic domains for $\epsilon = -4.4\%$ is evident as bright spots at small q (within the red box) in the $S(q)$. (**B**) Top panels show particle configurations before and after a cooperative rearrangement during coalescence. After the move, the bond order values for particles labeled red and green swapped with the net result being the lateral growth of a pseudomorphic domain by 1σ. (**C** and **D**) $P(n)$ and $\langle n \rangle$ for various ϵ. In (C), $P(n)$ for $\epsilon > -3.5\%$ decayed exponentially. (**E**) Hierarchically organized structures realized by hybrid heteroepitaxy. (**F**) A closeup of (E) showing local strain-relief by stripe formation. In (F), particles in the pseudomorphic regions appear dark in transmission microscopy due to island growth on top of this layer.

the heteroepitaxy of particles with short-range attraction. Direct imaging has helped highlight the role of cooperative particle dynamics in heteroepitaxy. We have found that many of these new dynamical processes fundamentally alter mass transport and collude to result in the final 3D film morphology. Our findings are of immediate import to atomic and nanoparticle heteroepitaxy and suggest that cooperative processes should be explicitly considered in future theories and simulations of surface growth. Further, these processes are likely to play a role even during the surface reconstruction of noble metals (*13*). While we have restricted our attention to thin colloidal films, how strain-relief occurs in thicker films remains to be understood. Confocal microscopic imaging should make these measurements feasible. From an application perspective, we have demonstrated that self-assembly on strain-relief patterns, hitherto restricted to atomic systems, offers unparalleled opportunities in the fabrication of defect-free surface structures made of larger particles as well. Expanding on our approach to include complex colloids can help circumvent kinetic bottlenecks that often plague their self-assembly and also aid in substrate-induced polymorph selection (*46*). Last, considering the observed overarching similarities in heteroepitaxial processes across particle size scales, the stage is now set for a meaningful dialog between the fields of atomic, nanoparticle, and colloidal heteroepitaxy.

MATERIALS AND METHODS

Our experimental system composed of charged-stabilized polystyrene colloids (diameter, $\sigma = 1$ μm; volume fraction, $\phi = 2.6\%$; Polysicence USA) and nonadsorbing polymer sodium carboxylmethyl cellulose (NaCMC; radius of gyration, $R_g \approx 50$ nm; mol. wt., 700 K; Fisher Scientific) as the depletant. The colloidal particles (volume fraction, $\phi = 0.13\%$) were sedimented on lithographically patterned (100) surfaces in the presence of NaCMC (concentration, 0.05 mg/ml). The polymers induced a short-ranged depletion attraction between the colloids and between the colloids and the substrate. We first determined the intrinsic lattice constant of the colloidal films, a_f, by letting the particles crystallize on a featureless surface. The equilibrium lattice constant was taken to be the first peak of the pair correlation function $g(r)$. Subsequently, we fabricated (100) substrates of the desired lattice periodicity, a_s, using the replica-imprinting technique (*19*, *33*). First, a linear array of trenches from a blazed diffraction grating (1200 lines/mm; blazed angle, 36.8°; Thorlabs) was transferred to a 1-mm-thick layer of polydimethylsiloxane (PDMS; SYLGARD 184). The PDMS film was then stretched uniaxially to the desired lattice spacing a_s. Next, the grating pattern on PDMS was transferred to an ultraviolet (UV)–curable optical adhesive (Norland, #81), supported on a glass coverslip (#1 1/2, Electron Microscopy Sciences), which served as the hard master template for further imprinting processes. Subsequently, poly(methyl methacrylate) (PMMA)–anisole solution (SDFCL, 9% w/w) was spin coated on a cleaned glass coverslip at 1000 rpm and cured at 170°C for nearly 40 min to get a ~500-nm-thick film of PMMA. The linear grating pattern of the hard master template (UV adhesive), which was premaintained at temperature $T_1 \sim 126°C < T_g$, was transferred to the PMMA substrate. Here, T_g is the glass transition temperature of PMMA. The square patterns were realized by a subsequent second imprint, orthogonal to the first one, at temperature $T_2 \sim 122°C$ ($< T_1$). By varying a_s, we accessed a range of misfits that spanned from $\epsilon = -5.5\%$ (compressive strain) to $\epsilon = +5.5\%$ (tensile strain). Particles were imaged at 1 to 5 frames/s using a Foculus 234SB camera attached to a Leica DMI 6000B transmission optical microscope (objective, 100×; numerical aperture, 1.4). Particle tracking and analysis were done using standard and custom-written algorithms (*35*) in MATLAB and ImageJ.

SUPPLEMENTARY MATERIALS

Supplementary material for this article is available at http://advances.sciencemag.org/cgi/content/full/6/10/eaay8418/DC1

REFERENCES AND NOTES

1. C. Teichert, Self-organization of nanostructures in semiconductor heteroepitaxy. *Phys. Rep.* **365**, 335–432 (2002).
2. Z. Zhenyu, M. G. Lagally, *Morphological Organization in Epitaxial Growth and Removal* (World Scientific, Singapore, 1999).
3. R. Nötzel, J. Temmyo, T. Tamamura, Self-organized growth of strained InGaAs quantum disks. *Nature* **369**, 131–133 (1994).
4. H. Brune, M. Giovannini, K. Bromann, K. Kern, Self-organized growth of nanostructure arrays on strain-relief patterns. *Nature* **394**, 451–453 (1998).
5. V. A. Shchukin, D. Bimberg, Spontaneous ordering of nanostructures on crystal surfaces. *Rev. Mod. Phys.* **71**, 1125 (1999).
6. K. Bromann, H. Brune, H. Röder, K. Kern, Interlayer mass transport in homoepitaxial and heteroepitaxial metal growth. *Phys. Rev. Lett.* **75**, 677–680 (1995).
7. H. Brune, K. Bromann, H. Röder, K. Kern, J. Jacobsen, P. Stoltze, K. Jacobsen, J. No, Effect of strain on surface diffusion and nucleation. *Phys. Rev. B* **52**, R14380–R14383 (1995).
8. M. Schroeder, D. E. Wolf, Diffusion on strained surfaces. *Surf. Sci.* **375**, 129–140 (1997).
9. Z. Zhang, M. G. Lagally, Atomistic processes in the early stages of thin-film growth. *Science* **276**, 377–383 (1997).

10. U. Kürpick, A. Kara, T. S. Rahman, Role of lattice vibrations in adatom diffusion. *Phys. Rev. Lett.* **78**, 1086–1089 (1997).
11. H. Brune, Microscopic view of epitaxial metal growth: Nucleation and aggregation. *Surf. Sci. Rep.* **31**, 125–229 (1998).
12. G. Springholz, V. Holy, M. Pinczolits, G. Bauer, Self-organized growth of three-dimensional quantum-dot crystals with fcc-like stacking and a tunable lattice constant. *Science* **282**, 734–737 (1998).
13. J. V. Barth, G. Costantini, K. Kern, Engineering atomic and molecular nanostructures at surfaces. *Nature* **437**, 671–679 (2005).
14. K. Aït-Mansour, M. E. Cañas-Ventura, P. Ruffieux, R. Jaafar, M. Bieri, R. Rieger, K. Müllen, R. Fasel, O. Gröning, Strain-relief pattern as guide for the formation of surface-supported bimolecular nanoribbons. *Appl. Phys. Lett.* **95**, 143111 (2009).
15. S. L. Hellstrom, Y. Kim, J. S. Fakonas, A. J. Senesi, R. J. Macfarlane, C. A. Mirkin, H. A. Atwater, Epitaxial growth of DNA-assembled nanoparticle superlattices on patterned substrates. *Nano Lett.* **13**, 6084–6090 (2013).
16. M. X. Wang, S. E. Seo, P. A. Gabrys, D. Fleischman, B. Lee, Y. Kim, H. A. Atwater, R. J. Macfarlane, C. A. Mirkin, Epitaxy: Programmable atom equivalents versus atoms. *ACS Nano* **11**, 180–185 (2016).
17. P. A. Gabrys, S. E. Seo, M. X. Wang, E. Oh, R. J. Macfarlane, C. A. Mirkin, Lattice mismatch in crystalline nanoparticle thin films. *Nano Lett.* **18**, 579–585 (2017).
18. A. van Blaaderen, R. Ruel, P. Wiltzius, Template-directed colloidal crystallization. *Nature* **385**, 321–324 (1997).
19. K. H. Lin, J. C. Crocker, V. Prasad, A. Schofield, D. A. Weitz, T. C. Lubensky, A. G. Yodh, Entropically driven colloidal crystallization on patterned surfaces. *Phys. Rev. Lett.* **85**, 1770–1773 (2000).
20. R. Ganapathy, M. R. Buckley, S. J. Gerbode, I. Cohen, Direct measurements of island growth and step-edge barriers in colloidal epitaxy. *Science* **327**, 445–448 (2010).
21. J. R. Savage, S. F. Hopp, R. Ganapathy, S. J. Gerbode, A. Heuer, I. Cohen, Entropy-driven crystal formation on highly strained substrates. *Proc. Natl. Acad. Sci. U.S.A.* **110**, 9301–9304 (2013).
22. N. Vogel, M. Retsch, C. A. Fustin, A. del Campo, U. Jonas, Advances in colloidal assembly: The design of structure and hierarchy in two and three dimensions. *Chem. Rev.* **115**, 6265–6311 (2015).
23. C. K. Mishra, A. K. Sood, R. Ganapathy, Site-specific colloidal crystal nucleation by template-enhanced particle transport. *Proc. Natl. Acad. Sci. U.S.A.* **113**, 12094–12098 (2016).
24. V. J. Anderson, H. N. Lekkerkerker, Insights into phase transition kinetics from colloid science. *Nature* **416**, 811–815 (2002).
25. Q. Chen, S. C. Bae, S. Granick, Directed self-assembly of a colloidal kagome lattice. *Nature* **469**, 381–384 (2011).
26. G. Meng, J. Paulose, D. R. Nelson, V. N. Manoharan, Elastic instability of a crystal growing on a curved surface. *Science* **343**, 634–637 (2014).
27. S. Bommel, N. Kleppmann, C. Weber, H. Spranger, P. Schäfer, J. Novak, S. V. Roth, F. Schreiber, S. H. L. Klapp, S. Kowarik, Unravelling the multilayer growth of the fullerene C60 in real time. *Nat. Commun.* **5**, 5388 (2014).
28. K. H. Nagamanasa, S. Gokhale, A. K. Sood, R. Ganapathy, Direct measurements of growing amorphous order and non-monotonic dynamic correlations in a colloidal glass-former. *Nat. Phys.* **11**, 403–408 (2015).
29. A. M. Alsayed, M. F. Islam, J. Zhang, P. J. Collings, A. G. Yodh, Premelting at defects within bulk colloidal crystals. *Science* **309**, 1207–1210 (2005).
30. B. Li, F. Wang, D. Zhou, Y. Peng, R. Ni, Y. Han, Modes of surface premelting in colloidal crystals composed of attractive particles. *Nature* **531**, 485–488 (2016).
31. P. Schall, I. Cohen, D. A. Weitz, F. Spaepen, Visualization of dislocation dynamics in colloidal crystals. *Science* **305**, 1944–1948 (2004).
32. Y. Peng, F. Wang, Z. Wang, A. M. Alsayed, Z. Zhang, A. G. Yodh, Y. Han, Two-step nucleation mechanism in solid-solid phase transitions. *Nat. Mater.* **14**, 101–108 (2015).
33. Y. Xia, E. Kim, X. M. Zhao, J. A. Rogers, M. Prentiss, G. M. Whitesides, Complex optical surfaces formed by replica molding against elastomeric masters. *Science* **273**, 347–349 (1996).
34. B. Müller, B. Fischer, L. Nedelmann, A. Fricke, K. Kern, Strain relief at metal interfaces with square symmetry. *Phys. Rev. Lett.* **76**, 2358–2361 (1996).
35. J. C. Crocker, D. G. Grier, Methods of digital video microscopy for colloidal studies. *J. Colloid Interface Sci.* **179**, 298–310 (1996).
36. E. Penev, P. Kratzer, M. Scheffler, Effect of strain on surface diffusion in semiconductor heteroepitaxy. *Phys. Rev. B* **64**, 085401 (2001).
37. C. Goyhenex, H. Bulou, J. P. Deville, G. Tréglia, Compressive strain versus tensile strain: A theoretical study of Pt/Co(0 0 0 1) and Co/Pt(1 1 1). *Appl. Surf. Sci.* **177**, 238–242 (2001).
38. P. Bak, Commensurate phases, incommensurate phases and the devil's staircase. *Rep. Prog. Phys.* **45**, 587–629 (1982).
39. G. Antczak, G. Ehrlich, Jump processes in surface diffusion. *Surf. Sci. Rep.* **62**, 39–61 (2007).
40. G. L. Kellogg, P. J. Feibelman, Surface self-diffusion on Pt (001) by an atomic exchange mechanism. *Phys. Rev. Lett.* **64**, 3143–3146 (1990).
41. G. Polya, About a task of the probability calculation concerning the random walk in the road network. *Math. Ann.* **84**, 149–160 (1921).
42. J. Tersoff, A. D. van der Gon, R. M. Tromp, Critical island size for layer-by-layer growth. *Phys. Rev. Lett.* **72**, 266–269 (1994).
43. D. G. Sangiovanni, A. B. Mei, D. Edström, L. Hultman, V. Chirita, I. Petrov, J. E. Greene, Effects of surface vibrations on interlayer mass transport: Ab initio molecular dynamics investigation of Ti adatom descent pathways and rates from TiN/TiN(001) islands. *Phys. Rev. B* **97**, 035406 (2018).
44. P. Ruggerone, C. Ratsch, M. Scheffler, Chapter 13 density-functional theory of epitaxial growth of metals. *Chem. Phys. Sol. Surf.* **8**, 490–544 (1997).
45. J. Park, D.-K. Kim, H.-N. Kim, C. J. Wang, M. K. Kwak, E. Hur, K. Suh, S. S. An, A. Levchenko, Directed migration of cancer cells guided by the graded texture of the underlying matrix. *Nat. Mater.* **15**, 792–801 (2016).
46. S. Arai, H. Tanaka, Surface-assisted single-crystal formation of charged colloids. *Nat. Phys.* **13**, 503–509 (2017).
47. B. I. Halperin, D. R. Nelson, Theory of two-dimensional melting. *Phys. Rev. Lett.* **41**, 121–124 (1978).
48. M. El-Batanouny, S. Burdick, K. M. Martini, P. Stancioff, Double-sine-Gordon solitons: A model for misfit dislocations on the Au (111) reconstructed surface. *Phys. Rev. Lett.* **58**, 2762–2765 (1987).
49. M. Mansfield, R. J. Needs, Application of the Frenkel-Kontorova model to surface reconstructions. *J. Phys. Condens. Matter* **2**, 2361–2374 (1990).
50. S. Mehendale, M. Marathe, Y. Girard, V. Repain, C. Chacon, J. Lagoute, S. Rousset, S. Narasimhan, Prediction of reconstruction in heteroepitaxial systems using the Frenkel-Kontorova model. *Phys. Rev. B* **84**, 195458 (2011).
51. X.-G. Ma, P.-Y. Lai, P. Tong, Colloidal diffusion over a periodic energy landscape. *Soft Matter* **9**, 8826–8836 (2013).

Acknowledgments: M.M. thanks UGC-CSIR for a research fellowship. A.K.S. thanks the Department of Science and Technology (DST), government of India for a Year of Science Fellowship. M.M. and R.G. thank the Ganapathy laboratory members for feedback on the manuscript. **Funding:** R.G. thanks DST-Nano Mission (SR/NM/TP-25/2016) and DST SwarnaJayanti (DST/SJF/PSA-03/2015-16) fellowship for financial support. **Author contributions:** R.G. initiated the research. M.M., C.K.M., A.K.S., and R.G. contributed to project development. M.M. performed experiments and carried out the data analysis. R.B. and S.N. performed the numerical analysis. M.M. and R.G. wrote the paper with inputs from all authors. **Competing interests:** The authors declare that they have no competing interests. **Data and materials availability:** All data needed to evaluate the conclusions in the paper are present in the paper and/or the Supplementary Materials. Additional data related to this paper may be requested from the authors.

Submitted 23 July 2019
Accepted 11 December 2019
Published 4 March 2020
10.1126/sciadv.aay8418

Citation: M. Mondal, C. K. Mishra, R. Banerjee, S. Narasimhan, A. K. Sood, R. Ganapathy, Cooperative particle rearrangements facilitate the self-organized growth of colloidal crystal arrays on strain-relief patterns. *Sci. Adv.* **6**, eaay8418 (2020).